Turkish Journal of Physics

Volume 48 | Number 2 Article 2

2024

Lithography-free highly sensitive detection of glucose based on colloidal spheres

Habibe Durmaz
Karamanoglu Mehmetbey University: Karamanoglu Mehmetbey Universitesi

TÜBİTAK

Turkish Journal of Physics

http://journals.tubitak.gov.tr/physics/

Research Article

Turk J Phys
(2024) 48: 40 – 49

doi:10.55730/1300-0101.2756

Lithography-free highly sensitive detection of glucose based on colloidal spheres

Habibe DURMAZ*
Department of Electrical and Electronics Engineering, Karamanoğlu Mehmetbey University, Karaman, Turkiye

Received: 01.01.2024 • **Accepted/Published Online:** 01.04.2024 • **Final Version:** 05.04.2024

Abstract: Diabetes has emerged as a global health crisis, with a substantial increase in prevalence and associated healthcare costs. The urgency for early diagnosis to prevent complications has fueled research into advanced biosensing technologies. Plasmonic sensors, leveraging localized surface plasmon resonance (LSPR), have gained prominence for their sensitivity. This study explores a metamaterial-based sensor platform comprising nanospheres fabricated through colloidal lithography. A comprehensive numerical and experimental analysis of the designed metamaterial-based sensor is presented, focusing on the spectral response at the resonance frequency of 535 nm. Finite-difference time-domain (FDTD) simulations reveal the field and charge distributions, enabling a systematic exploration of geometric parameters' impact on absorption resonance. The chosen optimum parameters are validated experimentally, demonstrating excellent agreement between numerical predictions and experimental outcomes. The spectral shifts occurring in the absorption spectrum of the sensor have demonstrated the molecular detection capability of very low concentrations of glucose oxidase, such as 0.001 ppm. Our approach, offering a cost-effective alternative to common fabrication methods, holds promise for the mass production of highly sensitive biosensors, providing a pathway for the development of advanced diagnostic tools for diabetes and other healthcare applications.

Key words: Colloidal lithography, glucose detection, plasmonic sensor

1. Introduction

Diabetes is a widespread chronic disease among the fastest-growing global health emergencies of the 21^{st} century. Five hundred and thirty-seven million adult individuals (aged 20–79) were reported living with diabetes and it has been estimated that this number will rise to 643 million in 2030 and 783 million in 2045 according to the International Diabetes Federation†. Diabetes† is responsible for 6.7 million deaths in 2021 in low- and middle-income countries. The healthcare expenditures for this disease amount to at least 996 billion dollars, indicating a 316% increase in spending over the past 15 years. Globally, 541 million adults have Impaired Glucose Tolerance (IGT)†, which puts them at high risk of developing type 2 diabetes. Diabetes Mellitus can be distinguished by the amount of increase in blood sugar levels resulting from disorders in insulin secretion or insulin action [1, 2]. High blood sugar, also known as glucose level, is directly associated with various health problems such as chronic kidney failure, cardiovascular diseases, stroke, retinal damage, and foot ulcers [3, 4]. The abnormal changes in glucose levels lead to life-threatening complications when examining these negative outcomes. Early diagnosis is crucial to prevent complications and reduce mortality. Recent studies have intensively focused on detecting glucose concentration with various methods, including electrochemical, colorimetric, optical, and thermoelectric-based biosensors [5–11].

*Correspondence: hdurmaz@kmu.edu.tr
†According to https://diabetesatlas.org

The working principles of the sensors used in research are quite different from others, and the selection of the most suitable sensor type is often based on performance, cost, and application areas. Among these sensor platforms, plasmonic sensors have smaller sizes and are more advantageous as they can operate at room temperature compared to others. In recent years, plasmonic sensors have attracted significant interest in developing new miniature devices in modern and advanced applications, including nano-antennas, gas generators, waveguides, and modulators [12–17]. Plasmonic biosensors work based on localized surface plasmon resonance (LSPR) as a result of electromagnetic radiation and produce strong resonance signals. The spectral response and signal strength of resonance mode are related to different results depending on the changes in the refractive index of the surrounding dielectric medium caused by the presence of the targeted analytes [14, 18–20].

Researchers have been conducting intensive studies to develop small-sized plasmonic sensors for the detection of various target analytes (biomolecules, gases, etc.). According to recent studies, plasmonic sensors are the most useful method for highly sensitive detection of biomolecules [18, 21–25]. These sensors are developed based on metamaterials that have ideal properties at microcellular dimensions compared to the wavelengths of the electromagnetic spectrum. These materials can achieve maximum power transfer and absorb light perfectly by matching the impedance of the material to the surrounding space $z = \sqrt{\frac{\mu}{\epsilon}} = 1$ by adjusting the geometric parameters of the selected material and its geometry (subnanostructures) in proper portions resulting in strong absorption across a wide electromagnetic spectrum.

Nanostructures have desired optical properties such as optical invisibility, strong near-field enhancement, and negative refractive index. These nanostructures have been extensively studied in biological and chemical sensors due to their advantages [26–28], nonlinear optics [29, 30], plasmonic photocatalysis [31, 32], waveguides [33, 34], and energy harvesting [35–37]. Most MAs consist of different unit cells and sizes of nanostructures or complex metal patterns [38–41]. The common fabrication of these sensors is costly and complex processes, such as electron beam lithography and ion beam etching. On the other hand, colloidal lithography offers a low-cost and suitable approach for the mass production of sensors although the periodicity and uniformity of optically designed sensors are not as perfect as those synthesized using lithography.

In this work, we have designed a plasmonic-based sensor platform consisting of nanospheres that are fabricated based on colloidal lithography. We have investigated the spectral response of the proposed sensor platform both numerically and experimentally. The numerical analysis including the field and charge distributions at the resonance frequency of 535 nm is carried out using the finite-difference time-domain (FDTD) method. The effect of geometric parameters on the absorption resonance is investigated, numerically. The optimum parameter of the sphere is chosen for experimental validation. Our numerical and experimental results are in good agreement as shown in Figure 1b.

2. Material and methods

2.1. Numerical analysis numerical design of the sensor platform

The dimensions of gold-coated spheres, the period, and the thickness of the film layers were studied using the Finite Difference Time Domain (FDTD) method. The spectral behavior of the designed nano-sphere antennas was numerically investigated and analyzed. In the simulation, a unit cell of a sphere was repeated in $x-$ and $y-$directions under periodic boundary conditions and a perfectly matched layer was set for the $x-$direction. The full simulation region was evaluated with a 5 nm mesh setting. A plane wave was illuminated at 90° along the $z-$direction under perfectly matched layer boundary conditions. The incoming radiation was set along the $y-$direction. The simulation results of the proposed sensor platform showed a resonance peak at 535 nm wavelength which is in good agreement with the experimental result.

The proposed sensor system is composed of gold-coated polystyrene spheres on a 140 nm thin layer of Si_3N_4 film on a glass substrate as shown in the schematic in Figure 2a. Inserting the Si_3N_4 interlayer, which is a high-index dielectric material, between the gold layer and the substrate will provide well well-defined single resonance mode [43].

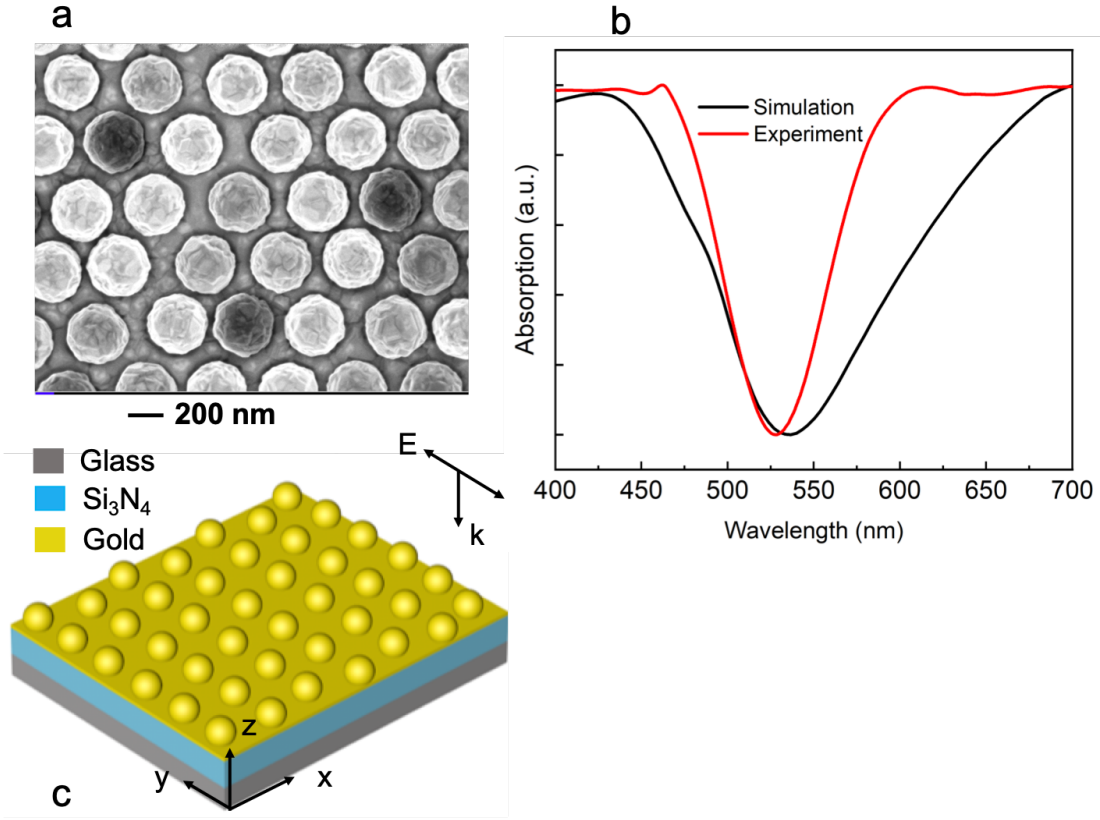

Figure 1. (a) SEM image of the structure of the gold-coated sphere. (b) Comparison of numerical and experimental absorption spectra of the plasmonic structure. The numerical absorption spectrum is obtained with FDTD simulation. The diameter of the polystyrene spheres is 240 nm, the thickness of the Si_3N_4 and gold layers are 140 nm and 60 nm, respectively.(c) The schematic view of the sensor platform. The electric field is oriented along the y-direction and k is the propagation direction of the incoming light.

The spectral response of the gold-coated spheres is at the wavelength of 535 nm as shown in Figure 2. By varying the diameter of the spheres, the resonance wavelength can be tuned to the desired frequency value. The strongest absorption was obtained for the sphere with 240 nm diameter and these parameters were used for the fabrication of the sensor platform for efficient results as seen in Figure 2. Also, the experimental result has a smaller full-width half maximum (FWHM) (63.7 nm) compared to the numerical result (108 nm). Having a smaller FWHM is a critical measure for the highly sensitive detection of analytes. The limit of detection (LOD) of plasmonics sensor, which is the smallest amount of analyte that plasmonic sensors can detect, is defined by sensitivity (S) and figure of merit (FoM). The sensitivity is calculated using the formula $S = \Delta\lambda/\Delta n$, which takes into account the shift in the resonance wavelength as the refractive index changes. The unit of sensitivity is the nm/refractive index unit (RIU). FoM $= S/\text{FWHM}$ value is obtained by dividing this sensitivity by the full-width at half-maximum of the resonance peak. As a result, the sensitivity of the sensor will increase with a low FoM value [42]. The sensitivity and FoM of our sensor are 3.75 nm/RIU and 0.058 RIU^{-1}, respectively.

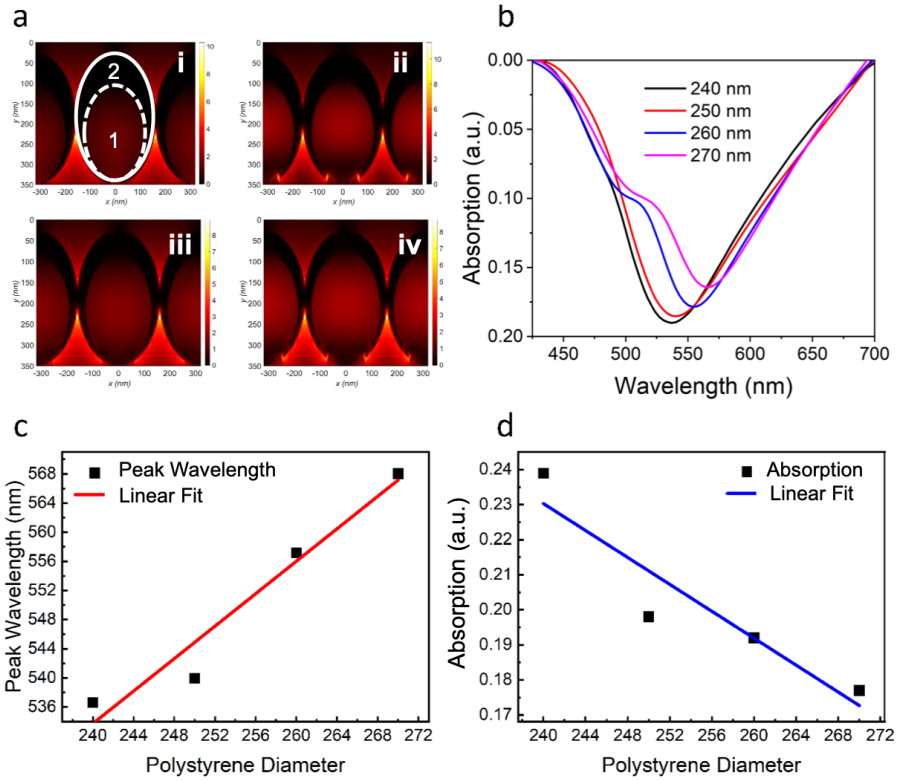

Figure 2. The enhanced electric field at gold-polystyrene spheres as the diameters of polystyrene spheres; i= 240 nm, ii= 250 nm, iii=260 nm, and iv= 270 nm. (b) The corresponding numerical absorption spectra (c) A linear relation between the resonance wavelength and the diameters of the polystyrene spheres. (d) Similarly, a linear relationship between the absorption rate and the diameters of the polystyrene spheres.

The difference between experimental and numerical data arises from the inability to precisely control the thickness of gold on the side walls of the 60 nm gold-coated spheres and the challenge of accurately applying this condition to the model provided in the simulation. In Figure 2a, the regions numbered 1 and 2 are the polystyrene and gold-covered regions, respectively. In the experiment, it is hard to know the thickness of the gold at the side wall of the polystyrene sphere. In addition, as the sensor system is experimentally formed by placing spheres on the surface using the colloidal method, the difficulty in controlling the periodic arrangement of the spheres contributes to the difference between experimental and numerical spectral responses.

The spectral responses were analyzed with the same program by varying the diameters of polystyrene spheres to determine the optimum absorption signal of the sensor platform. Figure 2a shows the electric field distributions of polystyrene spheres with diameters of 240, 250, 260, and 270 nm, respectively. According to this figure, as the diameter of the polystyrene sphere decreased, the development of the electric field increased. The stronger field confinement between the polystyrene spheres with a diameter of 240 nm and the gold layer was observed. The field confinement developed by the polystyrene spheres with a diameter of 240 nm exhibited a high absorption while the polystyrene spheres with a diameter of 270 nm showed a lower absorption signal. It is noted that the absorption strength increases as the diameter of the spheres gets smaller since the thin gold layer induces the excitation of surface plasmons at the interface between the polystyrene sphere and the gold layer. The maximum absorption strength for the sphere with a diameter of 240 nm is because the light-metal interactions couple to surface plasmons at 535 nm of the resonance frequency. As the diameter gets smaller than 240 nm (not shown here), absorption starts to decrease again as the impedance matching condition deteriorates. Also, as the diameter of the spheres gets smaller, the gap between the spheres increases; therefore, the light

transmission increases with a decrease in absorption. There is a linear dependence between the diameter of the sphere and the resonance wavelength as depicted in Figure 2c. The absorption rate is also linearly dependent on the diameter of the spheres as shown in Figure 2d. The linear relationship in these results is crucial for obtaining repeatable and reliable results in plasmonic sensor designs. Also, it gives insight to understand the sensitivity and specificity of the sensors.

The localized near-electric field enhancement between the gold layer and the polystyrene spheres at the resonance wavelength is given in Figure 2a side view and Figure 3a top view. The interaction of light with the gold-coated spheres triggers the excitation of localized surface plasmons (LSPs), which are collective oscillations of conduction electrons responding to the incident electromagnetic fields. Particularly, regions between the polystyrene spheres and the gold layer experience significant increases in localized electric fields due to the excitation of LSPs resulting from near-field interactions of densely packed polystyrene spheres. The interaction between closely positioned spheres results in the generation of dipole moments with opposite charges relative to their neighboring dipoles as shown in Figure 3b resulting in the formation of a complex pattern characterized by varying charge polarization. The charge exchange between the polystyrene and gold layers occurs due to the dynamic dipole moment of the subwavelength particles resulting in the generation of an electric current at the resonance wavelength. This generated current induces a magnetic field that is one of the criteria for satisfying the impedance matching along with the electric field at a specific resonance frequency.

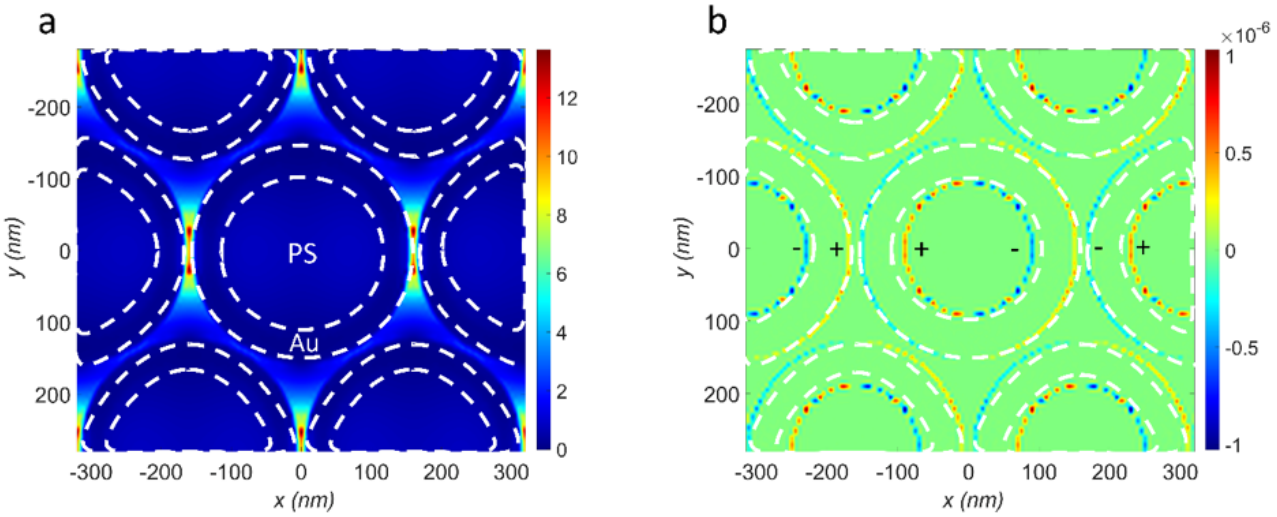

Figure 3. (a) The enhancement of the electric field between the gold layer and the polystyrene spheres at the resonance wavelength of 535 nm. (b) The dipolar charge distributions on the surface at the resonance wavelength of 535 nm.

3. Experimental analyses of the sensor platform

3.1. Fabrication process

The glass-based chip 2.5×2.5 cm^2 is washed with acetone, ethanol, and deionized (DI) water in a 5-min ultrasonic bath, followed by drying with dry air. After drying, it is treated with a UV-Ozone cleaning device to remove any remaining organic residues from the surface. Subsequently, as shown in Figure 4b, it is coated with a silicon nitride (Si_3N_4) film with a thickness of 140 nm using electron-beam evaporation. The coating process is optimized to achieve a homogeneous film formation at a rate of 1 kÅ/s. Once the film structure is obtained, hydrophilic polystyrene colloidal spheres (PS) with carboxyl groups and dimensions of 0.5 μm are coated onto the surface using dip-coating and Langmuir–Blodgett techniques at the air/water interface

(Figure 4c). The formation of a monolayer coating relies on the principle of a hexagonal close-packed (HCP) arrangement of colloidal polystyrene spheres on the surface. The tightly packed monolayer has almost no gaps between the spheres (Figure 4c). This characteristic ensures that the subsequent coating on the monolayer is closely aligned with the thin film formation, without forming plasmonic hotspots. Therefore, a pretreatment process is performed to enhance the plasmonic behavior of the polystyrene sphere template, referred to as size reduction. In this process, reactive ion etching (RIE) is employed to create spaces between the spheres without disrupting their periodic arrangement (Figure 4d). These spaces facilitate the formation of points that positively influence plasmonic behavior during the subsequent gold coating. After reducing the sizes of the spheres within the desired ranges, the gold coating is applied using the thermal deposition method (Figure 4e). The resulting chip consists of gold-coated spheres on the surface as depicted in the SEM image in Figure 1a.

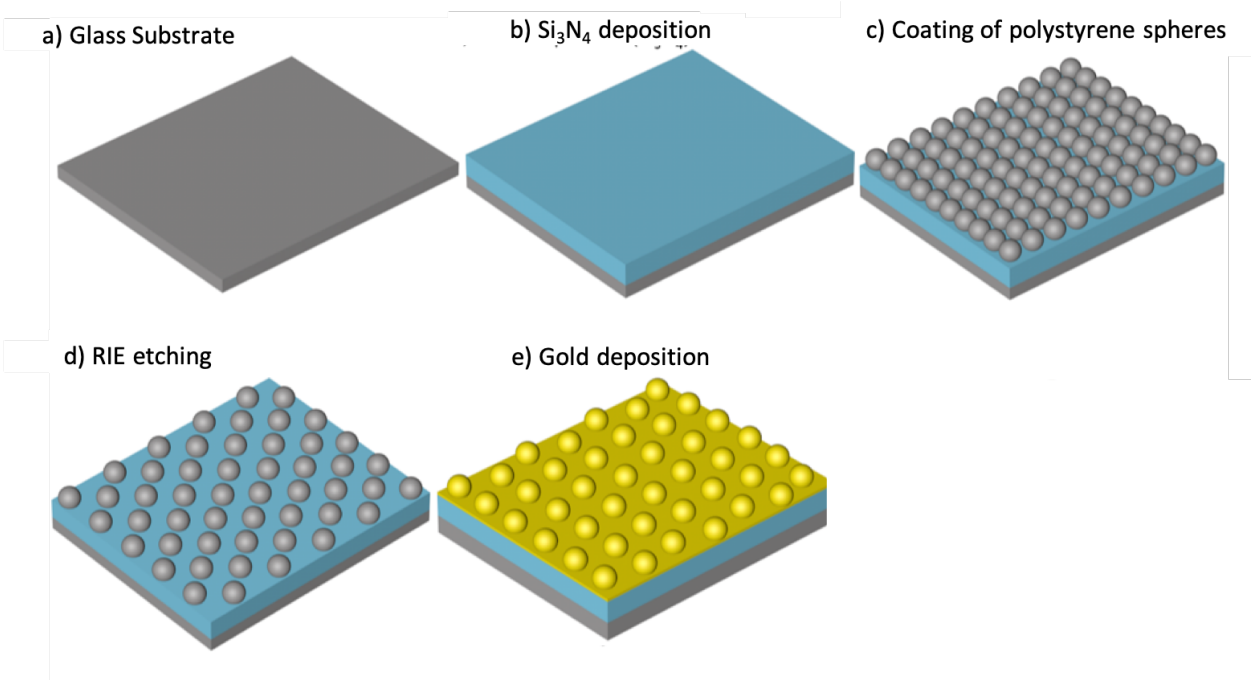

Figure 4. Schematic of plasmonic-based biosensor fabrication. (a) Silicon nitride (Si_3N_4) deposition on the glass substrate using electron-beam evaporation. (b) Coating of polystyrene spheres onto the Si_3N_4-coated substrate in a monolayer hexagonal close-packed formation. (c) Opening up spaces between the polystyrene spheres using the size reduction method with RIE. (d) Thermal deposition of gold onto the polystyrene template to obtain plasmonic structures. The thickness of the Si_3N_4 and gold layers are 140 nm and 60 nm, respectively.

3.2. Validation of the detection of the glucose

To validate the detection capabilities of the proposed plasmonic sensor, different concentrations of glucose oxidase ranging from 0.001 ppm to 0.5 ppm were prepared. 10 mg of glucose oxidase was diluted in 10 mL of buffer oxide solution to create a 1000 ppm solution stock. For the assessment of the sensitivity of the proposed sensor platform, buffer oxide solution was added to get at concentrations of 0.001, 0.005, 0.01, 0.05, and 0.5 ppm. Initially, a bare spectrum without any analyte on the sensor surface was recorded with 0.1 nm resolution for 128 sample points. Then the smallest concentration of 0.001 ppm was added carefully to the sensor surface with a micropipette and coated with spin-coat to cover the surface of the chip with a uniform film of glucose oxidase and let it dry at room temperature for 15 min before taking the spectrum.

The experimental setup was composed of the sensor chip integrated with a visible spectrometer (Torr Lab OSA 20X, model CCS 200) equipped with an Ocean Optic halogen Light source to visualize the different concentrations of molecules. The experimental absorption spectra were recorded for different concentrations of each molecule as shown in Figure 5a. Initially, a reference spectrum (bare) in the air was recorded for background normalization then the spectrum from a bare sensor was recorded. The background normalization provided a clean pure spectral response from only the plasmonic sensor at the resonance wavelength. All the spectra were recorded starting from 0.001 ppm to 0.05 ppm for each molecule on identical chips.

There is a red-shift in resonance wavelength by approximately 5 nm with the 0.001 ppm concentration relative to the bare signal as shown in Figure 5a. A detailed examination of the resonance wavelength change with the concentration is shown in Figure 5b confirming a linear relation until the sensor surface is saturated.

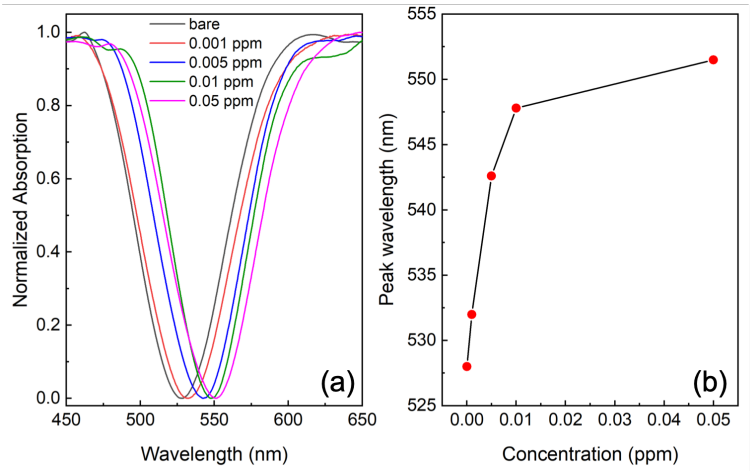

Figure 5. The experimental absorption spectra of the plasmonic sensor without glucose and with glucose at a concentration of 0.001 ppm to 0.05 ppm. (b) The spectral shift of glucose due to the concentration of 0.001 ppm to 0.05 ppm.

4. Conclusion

In this study, the detection of glucose oxidase was aimed at using a highly sensitive plasmonic sensor based on gold-coated polystyrene spheres. This sensor platform uses the cost-effective technique of colloidal lithography, enabling the detection of glucose at a remarkably low concentration of 0.001 ppm. The results showed a spectral shift of 5 nm at the resonance frequency at 0.001 ppm concentration, enabling molecular detection with a sensitivity of $\sim$3.75 nm/RIU and FoM of $\sim$0.058 RIU^{-1}.The developed plasmonic sensor platform provides sensitive detection without requiring complicated set-up and specialized personnel. Experimental results demonstrate that an enzyme-free, simple, and portable plasmonic sensor can detect glucose at the lowest concentration of 0.001 ppm. The developed sensor platform can be used as a detection tool for biological and chemical substances in defense and health applications. Our results can provide valuable perspectives for fundamental research and present significant benefits for practical implementations. This sensor platform can be improved by adding surface modification via molecule bindings for the detection of certain analytes in complex solutions for defense and biochemical applications. In light of this data, it enhances our understanding of the potential impact of plasmonic devices and sensors on forthcoming research and applications.

Acknowledgment

We would like to thank Karamanoğlu Mehmetbey University and Bilkent University UNAM facility for their support in the conduct of this study.

References

[1] Türkiye Diyabet Vakfı, "TÜRKDİAB Diyabet Tanı ve Tedavi Rehberi 2019," *Ulusal Diyabet Konsensus Grubu*, 9. Baskı, Pasifik Reklam ve Tanıtım Hizmetleri, İstanbul (2019) (in Turkish).

[2] Çocuk Endokrinolojisi ve Diyabet Derneği, "Çocukluk Çağı Diyabeti: Tanı ve Tedavi Rehberi 2018," *Ulusal Çocuk Diyabet Grubu*, Buluş Tasarım ve Matbaacılık Hizmetleri, Ankara (2018) (in Turkish).

[3] Y. Marunaka, "Roles of interstitial fluid pH in diabetes mellitus: Glycolysis and mitochondrial function," *World J Diabetes* **6(1)** (2015) 125–135.

[4] C. P. Domingueti, L. M. S. A. Dusse, M. D. G. Carvalho, L. P. de Sousa, K. B. Gomes, and A. P. Fernandes, "Diabetes mellitus: The linkage between oxidative stress, inflammation, hypercoagulability and vascular complications," *J. Diabetes Complications* **30(4)** (2016) 738–745.

[5] M. A. Akhtar, R. Batool, A. Hayat, D. Han, S. Riaz, et al., "Functionalized Graphene Oxide Bridging between Enzyme and Au-Sputtered Screen-Printed Interface for Glucose Detection," *ACS Appl. Nano Mater.* **2** (2019) 1589–1596.

[6] R. Ahmad, M. Vaseem, N. Tripathy, and Y. B. Hahn, "Wide Linear-Range Detecting Nonenzymatic Glucose BiosensorBased on CuO Nanoparticles Inkjet-Printed on Electrodes," *Anal. Chem.* **85** (2013) 10448–10454.

[7] V. E. Coyle, A. E. Kandjani, M. R. Field, P. Hartley, M. Chen, et al., "Co_3O_4 needles on Au honeycomb as a non-invasive electrochemical biosensor for glucose in saliva," *Biosensors and Bioelectronics* **141** (2019) 111479.

[8] J. Xiao, Y. Liu, L. Su, D. Zhao, L. Zhao, and X. Zhang, "Microfluidic Chip-Based Wearable Colorimetric Sensor for Simpleand Facile Detection of Sweat Glucose," *Anal. Chem.* **91(23)** (2019) 14803–14807.

[9] R. Ahmad, M. Khan, M. R. Khan, N. Tripathy, M. I. R. Khan, et al., "Nano-donuts shaped nickel oxide nanostructures for sensitive non-enzymatic electrochemical detection of glucose," *Microsystem Technologies* **28** (2022) 313–318.

[10] W. Han, H. He, L. Zhang, C. Dong, H. Zeng, et al., "A Self-Powered Wearable Noninvasive Electronic-Skin forPerspiration Analysis Based on Piezo-Biosensing Unit Matrix of Enzyme/ZnO Nanoarrays," *ACS Appl. Mater. Interfaces* **9(35)** (2017) 29526–29537.

[11] R. Ahmad, M. Khan, N. Tripathy, M. I. R. Khan, and A. Khosla, "Hydrothermally Synthesized Nickel Oxide Nanosheets for Non-Enzymatic Electrochemical Glucose Detection," *J. Electrochem. Soc.* **167** (2020) 107504.

[12] Y. Kang, Y. Gong, Z. Hu, Z. Li, Z. Qiu, et al., "Plasmonic hot electron enhanced MoS_2 photocatalysis in hydrogen evolution," *Nanoscale* **7** (2015) 4482–4488.

[13] N. Liu, M. L. Tang, M. Hentschel, H. Giessen and A. P. Alivisatos, "Nanoantenna-enhanced gas sensing in a single tailored nanofocus," *Nature Materials* **10** (2011) 631–636.

[14] S. A. Maier, P. G. Kik, H. A. Atwater, S. Meltzer, E. Harel, et al., "Local detection of electromagnetic energy transport below the diffraction limit in metal nanoparticle plasmon waveguides," *Nature Materials* **2** (2003) 229–232.

[15] Z. Ma, M. H. Tahersima, S. Khan and V. J. Sorger, "Two-Dimensional Material-Based Mode Confinement Engineering in Electro-Optic Modulators," *IEEE Journal of Selected Topics in Quantum Electronics* **23** (2017) 81–88.

[16] M. P. Nielsen, X. Shi, P. Dichtl, S. A. Maier and R. F. Oulton, "Giant nonlinear response at a plasmonic nanofocus drives efficient four-wave mixing," *Science* **358** (2017) 1179–1181.

[17] A. Belushkin, F. Yesilkoy and H. Altug, "Nanoparticle-Enhanced Plasmonic Biosensorfor Digital Biomarker Detection in a Microarray," *ACS Nano* **12** (2018) 4453–4461.

[18] K. A. Willets and R. P. Van Duyne, "Localized Surface Plasmon Resonance Spectroscopy and Sensing," *Annu. Rev. Phys. Chem.* **58** (2007) 267–297.

[19] C. Genet and T. W. Ebbesen, "Light in tiny holes," *Nature* **445** (2007) 39–46.

[20] Z. Fang, Y.-R. Zhen, L. Fan, X. Zhu and P. Nordlander, "Tunable wide-angle plasmonic perfect absorber at visible frequencies," *Phys. Rev. B* **85** (2012) 245401.

[21] B. Mehta, K. D. Benkstein, S. Semancik and M. E. Zaghloul, "Gas Sensing with Bare and Graphene-covered Optical Nano-Antenna Structures," *Scientific Reports* **6** (2016) 21287.

[22] M. E. Stewart, C. R. Anderton, L. B. Thompson, J. Maria, S. K. Gray, et al., "Nanostructured Plasmonic Sensors," *Chem. Rev.* **108** (2008) 494–521.

[23] Y. Zhao, M. Zaghloul, Y. Lilach, K. Benkstein and S. Semancik, "Metal Organic Framework-Coated Optical VOC Gas Sensor," *2018 IEEE Photonics Conference (IPC)* (2018) 1–2.

[24] A. Tittl, H. Giessen and N. Liu, "Plasmonic gas and chemical sensing," *Nanophotonics* **3** (2014) 157–180.

[25] K. S. L. Al-Badri, " Multi Band Metamaterials Absorber for Stealth Applications," *Law, State and Telecommunications Review* **11** (2019) 133–144.

[26] S. D. Liu, X. Qi, W. C. Zhai, Z. H. Chen, W. J. Wang and J. B. Han, "Polarization state-based refractive index sensing with plasmonic nanostructures," *Nanoscale* **7** (2015) 20171.

[27] T. Allsop, R. Arif, R. Neal, K. Kalli, V. Kundrat, et al., "Photonic gas sensors exploiting directly the optical properties of hybrid carbon nanotube localized surface plasmon structures," *Light Sci. Appl.* **5** (2016) e16036.

[28] B. Park, S. H. Yun, C. Y. Cho, Y. C. Kim, J. C. Shin, et al., "Surface plasmon excitation in semitransparent inverted polymer photovoltaic devices and their applications as label-free optical sensors," *Light Sci. Appl.* **3** (2014) e222.

[29] M. A. Foster, A. C. Turner, M. Lipson and A. L. Gaeta, "Nonlinear optics in photonic nanowires," *Optics Express* **16** (2008) 1300–1320.

[30] P. Genevet, J. P. Tetienne, E. Gatzogiannis, R. Blanchard, M. A. Kats, et al., "Large Enhancement of Nonlinear Optical Phenomena by Plasmonic Nanocavity Gratings," *Nano Lett.* **10** (2010) 4880–4883.

[31] C. An, S. Peng and Y. Sun, "Facile synthesis of sunlight-driven AgCl: Ag plasmonic nanophotocatalyst," *Adv. Mater.* **22** (2010) 2570–2574.

[32] F. Pincella, K. Isozaki and K. Miki, "A visible light-driven plasmonic photocatalyst," *Light Sci. Appl.* **3** (2014) e133.

[33] R. F. Oulton, V. J. Sorger, D. A. Genov, D. F. P. Pile and X. Zhang, "A hybrid plasmonic waveguide for subwavelength confinement and long-range propagation," *Nature Photonics* **2** (2008) 496–500.

[34] L. Gao, L. Tang, F. Hu, R. Guo, X. Wang, and Z. Zhou, "Active metal strip hybrid plasmonic waveguide with low critical material gain," *Optics express* **20(10)** (2012) 11487-11495.

[35] Y. Qu, Q. Li, H. Gong, K. Du, S. Bai, et al., "Spatially and spectrally resolved narrowband optical absorber based on 2D grating nanostructures on metallic films," *Adv. Optical Mater.* **4** (2016) 480–486.

[36] J. Y. Lu, S. H. Nam, K. Wilke, A. Raza, Y. E. Lee, et al., "Localized Surface Plasmon-Enhanced Ultrathin Film Broadband Nanoporous Absorbers," *Adv. Optical Mater.* **4** (2016) 1255–1264.

[37] Q. Li, J. Gao, Z. Li, H. Yang, H. Liu, et al., "Absorption enhancement in nanostructured silicon fabricated by self-assembled nanosphere lithography," *Optical Materials* **70** (2017) 165-170.

[38] A. K. Azad, W. J. M. Kort-Kamp, M. Sykora, N. R. Weisse-Bernstein, T. S. Luk, et al., "Metasurface broadband solar absorber," *Scientific Reports* **6** (2016) 20347.

[39] S. Gu, B. Su, X. Zhao, "Planar isotropic broadband metamaterial absorber," *J. Appl. Phys.* **114** (2013) 163702.

[40] Y. Z. Cheng, Y. Wang, Y. Nie, R. Z. Gong, X. Xiong, X. Wang, "Design, fabrication and measurement of a broadband polarization-insensitive metamaterial absorber based on lumped elements," *J. Appl. Phys.* **111** (2012) 044902.

[41] C. Zhang, Q. Cheng, J. Yang, J. Zhao, T. J. Cui, "Broadband metamaterial for optical transparency and microwave absorption," *Appl. Phys. Lett.* **110** (2017) 143511.

[42] P. Offermans, C. M. Schaafsma, S. R. K. Rodriguez, Y. Zhang, M. Crego-Calama, S. H. Brongersma, J. Gomez Rivas, "Universal Scaling of the Figure of Merit of Plasmonic Sensors," *ACS Nano* **5** (2011) 5151-5157.

[43] A.E. Cetin, D. Etezadi, B. C. Galarreta, M. P. Busson, Y. Eksioglu, H. Altug,"Plasmonic Nanohole Arrays on a Robust Hybrid Substrate for Highly Sensitive Label-Free Biosensing," *ACS Photonics* **2** (2015) 1167–1174.